Temperature-Dependent Vibrational Modes in Sodium Nitrite*

M. K. BARNOSKI† AND J. M. BALLANTYNE
School of Electrical Engineering, Cornell University, Ithaca, New York 14850
(Received 28 May 1968)

The reflectivity of single-crystal sodium nitrite has been measured as a function of temperature and crystallographic orientation over a wavelength region which spans all the eight infrared-active normal modes. The temperature-dependent dielectric response functions and oscillator parameters have been obtained both by a Kramers-Kronig analysis and by fitting the reflectivity data with a series of independent harmonic oscillators. The latter model produces a good fit to the observed reflectivity at all temperatures both above and below the phase transition. Although all observed modes are temperature-dependent, none is thought to be a ferroelectric soft mode.

I. INTRODUCTION

SODIUM nitrite was discovered to be a ferroelectric in 1958 by Sawada and co-workers.[1] The transition from the paraelectric to ferroelectric phase occurs at approximately 163°C and is of the order-disorder type associated with the reorientation of NO_2^- radicals.[2] The behavior of the lattice dynamics of this substance in the vicinity of the ferroelectric transition temperature is of interest because of the possibility of the existence of "soft" ferroelectric modes.

Until most recently, the investigation of the infrared spectrum of $NaNO_2$ has largely been directed at location and assignment of the internal modes of vibration of the nitrite ion.[3–5] However in 1966, Vogt and Happ[6] recorded the temperature dependence of the polarized infrared reflectivity of the five lattice modes which occur in the 100 to 250-cm^{-1} spectral region. More recently, Axe[7] reported the dielectric dispersion of $NaNO_2$ obtained from a Kramers-Kronig analysis of the polarized room-temperature reflectivity.

As a result of the experiment to be reported herein, the temperature-dependent reflectivity is now known over the entire spectral region covering all eight infrared-active normal vibrations. In addition to the strong temperature dependence of the lattice vibrations which was observed by Vogt and Happ, it has been found that the reflectivity associated with the internal vibrations of the NO_2^- radical is also strongly temperature-dependent.

In 1966, Hatta[2] measured the temperature dependence of the dielectric constant at frequencies ranging from 5 MHz to 24 GHz at temperatures ranging from room temperature to 210°C. These measurements reveal that the dielectric constant obeys a Debye-type dispersion formula with a single relaxation time. This large low-frequency dispersion is most assuredly associated with the transition mechanism.

In order to determine the effect of the phase transition on the normal modes and to determine if any of the modes possess the characteristics of an unstable ferroelectric soft mode,[8] the reflectivity has been analyzed by employing both a Kramers-Kronig technique and by fitting it to the computed reflectivity of a set of independent harmonic oscillators.

II. SYMMETRY CONSIDERATIONS

The bravais lattice of the paraelectric phase is body centered orthorombic with one molecule per primitive unit cell. The hemihedral symmetry is the full holohedry of the lattice D_{2h}. The space group for this phase is D_{2h}^{25}.[9] For temperatures less than 163°C, the lattice remains body-centered orthorombic, but the hemihedral symmetry becomes C_{2v}, a subgroup of D_{2h}. The space group for the ferroelectric phase is C_{2v}^{20}. A standard group-theory analysis under a factor-group representation[10,11] of the ferroelectric space group (C_{2v}^{20}) reveals that in this phase the crystal possesses nine optical normal modes of vibration of which eight are infrared active. Of these eight modes, five are lattice vibrations of the sodium ions against the nitrite ions. The remaining three modes are the internal normal modes of the nitrite ion. Illustrative diagrams along with more detailed discussion of the various modes can be found in Refs. 6, 12, and 13. Table I lists the observed resonant frequencies, irreducible representations, and types of the infrared-active modes obtained at room temperature by various other authors.[5,7,12,14] The nomenclature of the irreducible representations of C_{2v} shown is consistent with the coordinate system used in Ref. 12.

* Research supported by the Advanced Research Projects Agency through the Materials Science Center, Cornell University.
† Present address: Honeywell Radiation Center, Boston, Mass.
[1] S. Sawada, S. Nomura, S. Fujii, and I. Yoshida, Phys. Rev. Letters **9**, 320 (1958).
[2] I. Hatta, T. Sakudo, and S. Sawada, J. Phys. Soc. Japan **21**, 1612 (1966).
[3] J. Sidman, J. Am. Chem. Soc. **79**, 2675 (1957).
[4] R. E. Weston and T. F. Brodasky, J. Chem. Phys. **27**, 683 (1957).
[5] R. Newman, J. Chem. Phys. **20**, 444 (1952).
[6] H. Vogt and H. Happ, Phys. Status Solidi **16**, 711 (1966).
[7] J. D. Axe, IBM Research Paper No. RC-1905, 1967 (unpublished); Bull. Am. Phys. Soc. **12**, 371 (1967).
[8] F. Jona and G. Shirane, *Ferroelectric Crystals* (Pergamon Press, Inc., New York, 1963).
[9] Y. Sato, K. Gesi, and Y. Takagi, J. Phys. Soc. Japan **16**, 2172 (1961).
[10] D. F. Hornig, J. Chem. Phys. **16**, 1063 (1948).
[11] H. Winston and R. S. Halford, J. Chem. Phys. **17**, 607 (1949).
[12] E. V. Chisler and M. S. Shur, Phys. Status Solidi **17**, 163 (1966).
[13] G. Herzberg, *Infrared and Raman Spectra* (D. Van Nostrand Co., Inc., Princeton, N. J., 1964).
[14] A. Tramer, Compt. Rend. **248**, 3546 (1959).

TABLE I. Room-temperature resonant frequencies and mode assignments for $NaNO_2$.

Irr. rep. of C_{2v}^{20}	Mode type and activity	Tramer[a,b] ν(cm^{-1})	Chisler and Shur[a,c] ν(cm^{-1})	Newman[d] ν(cm^{-1})	Axe[e] ν(cm^{-1})	This work ν(cm^{-1})	
A_1	trans. vib. $\bar{E}\|\bar{b}$	not obs.	not obs.	···	194	186	
A_2	rot. vib.	122	119	···	inactive	inactive	
B_1	trans. vib. $\bar{E}\|\bar{c}$	150–170	153	···	157	154	lattice
B_1	rot. vib. $\bar{E}\|\bar{c}$	185	177	···	188	187	modes
B_2	trans. vib. $\bar{E}\|\bar{a}$	148	not obs.	···	149	144	
B_2	rot. vib. $\bar{E}\|\bar{a}$	210–225	220	···	223	220	
A_1	sym. bend $\bar{E}\|\bar{b}$	828	825	831	826	825	
A_1	sym. stretch $\bar{E}\|\bar{b}$	1327	1327	1325	1323	1321	internal modes
B_1	asym. stretch $\bar{E}\|\bar{c}$	1230–1360	1239–1280	1360	1235	1223	

[a] Raman spectra. [b] Reference 14. [c] Reference 12. [d] Reference 5. [e] Reference 7.

III. EXPERIMENTAL TECHNIQUE

Single-crystal $NaNO_2$ was grown by solidification from the melt. After cleavage of the original piece, single crystals on the order of $3\times1\times1$ cm were often produced. Crystallographic orientations were easily obtainable from the cleaved pieces[15]; however, as a check, Laue back-reflection photographs were taken of some samples and analyzed. Samples in the desired crystallographic orientations were obtained by cutting the crystals on a chemical saw and subsequently polishing the spectral surface on a ground plate using a water and acetone solution.

Reflectivity measurements were made over the 10 to 60 cm^{-1} and 250 to 4000 cm^{-1} regions. In the 4000 to 250 cm^{-1} region a Perkin-Elmer 521 dual-beam infrared grating spectrophotometer equipped with a gold wire grid polarizer and microspecular reflectance attachment (angle of incidence 13°) was employed. The reflectance attachment was provided with a heatable sample mount whose temperature was controlled to within ±2°C, as monitored with a fine thermocouple in contact with the crystal surface.

Two different samples were used to achieve the three desired polarizations. One sample was prepared with a (010) spectral surface and a second with a (100) spectral surface. Thus, polarizations parallel to the a and c axes and parallel to the b and c axes were attainable. To check surface effects the reflectivity polarized parallel to the c axis was checked at various wavelengths using both samples. The values obtained agreed to within a few percent which was within the accuracy attainable when the samples were removed and repositioned. From repeated measurements, the estimated accuracy of the reflectivity is 2–5% over the entire spectral region at all temperatures considered.

[15] S. Nomura, Y. Asao, and S. Sawada, J. Phys. Soc. Japan **16**, 917 (1961).

In order to obtain access to the very far infrared portion of the spectrum, a lamellar grating interferometer similar to that described by Richards[16] was employed. The reflectivity attachment employed was of the conical type used by Ballantyne[17] and had an angle of incidence of 10°.

IV. EXPERIMENTAL RESULTS AND DETERMINATION OF DISPERSION PARAMETERS

Reflectivity was measured at several temperatures between 30 and 205°C over the entire available spectral region. Results at room temperature agreed closely with those of Axe.[7] The only differences were that the peak value of the reflectivities of three internal modes were found to be somewhat greater than those previously recorded while the widths of the two modes polarized parallel to the polar axis were found to be narrower. Figure 1 shows the reflectivity at 176°C for radiation polarized along the three crystallographic axes, and is representative of the results at other temperatures. The temperature dependencies of the various modes are shown in Figs. 2–4. The reflectivity in the 100–250 cm^{-1} region is that of Vogt and Happ.[6] Inspection reveals that all eight infrared-normal modes are temperature-dependent. In the 10 to 60 cm^{-1} region the reflectivity was found to be wavelength-independent and in agreement with the long-wavelength tails of Vogt and Happ[6] and the measured microwave values.[18]

Among the dispersion parameters of interest are the real and imaginary parts of the complex dielectric response function. Two methods were employed in their determination. A Kramers-Kronig analysis was performed first. In the second method the dielectric

[16] P. L. Richards, J. Opt. Soc. Am. **54**, 1474 (1964).
[17] J. M. Ballantyne, Phys. Rev. **136**, A429 (1964).
[18] E. Nakamura, J. Phys. Soc. Japan **17**, 961 (1962).

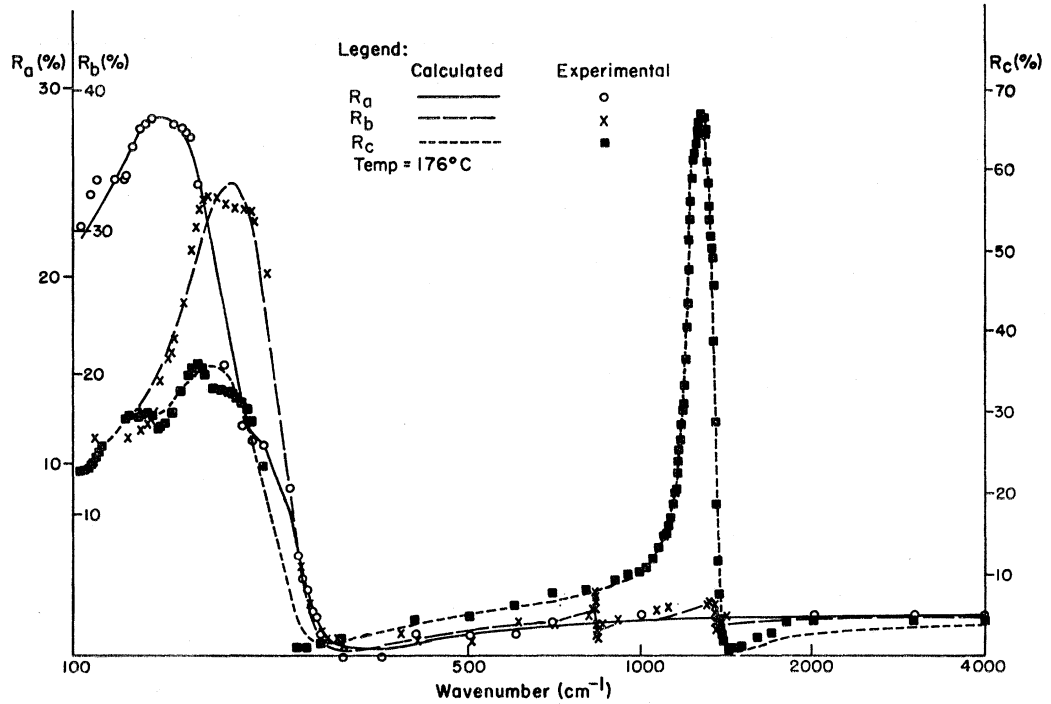

FIG. 1. Experimental and calculated reflectivity for radiation polarized along the three principal axes of a crystal at 176°C. The curves are calculated from an independent oscillator model while the points are experimental.

constant of the crystal was assumed to be that of a system of independent harmonic oscillators. The mode strengths, linewidths, and resonant frequencies characterizing such a system were then adjusted so that the reflectivity corresponding to such a system matched that obtained experimentally.

The integration and associated computations for the Kramers-Kronig analysis were accomplished using a program similar to one written by Ballantyne.[19] In this computation the Fresnel equation for normal incidence is used, since for angles of incidence on the order of 10° the error introduced by assuming normal incidence is

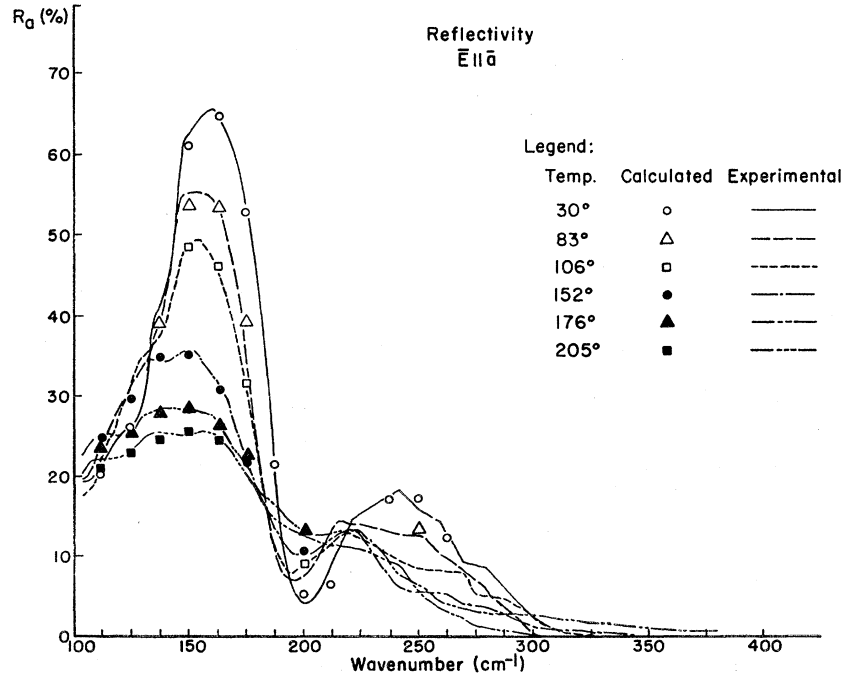

FIG. 2. Temperature-dependent reflectivity of the two a-axis lattice modes of type B_2. The curves are experimental and the points are those calculated from an independent oscillator model.

[19] B. B. East and W. B. Westphal (and J. M. Ballantyne), M.I.T. Technical Report No. 189, Lab. Ins. Res., 1964 (unpublished).

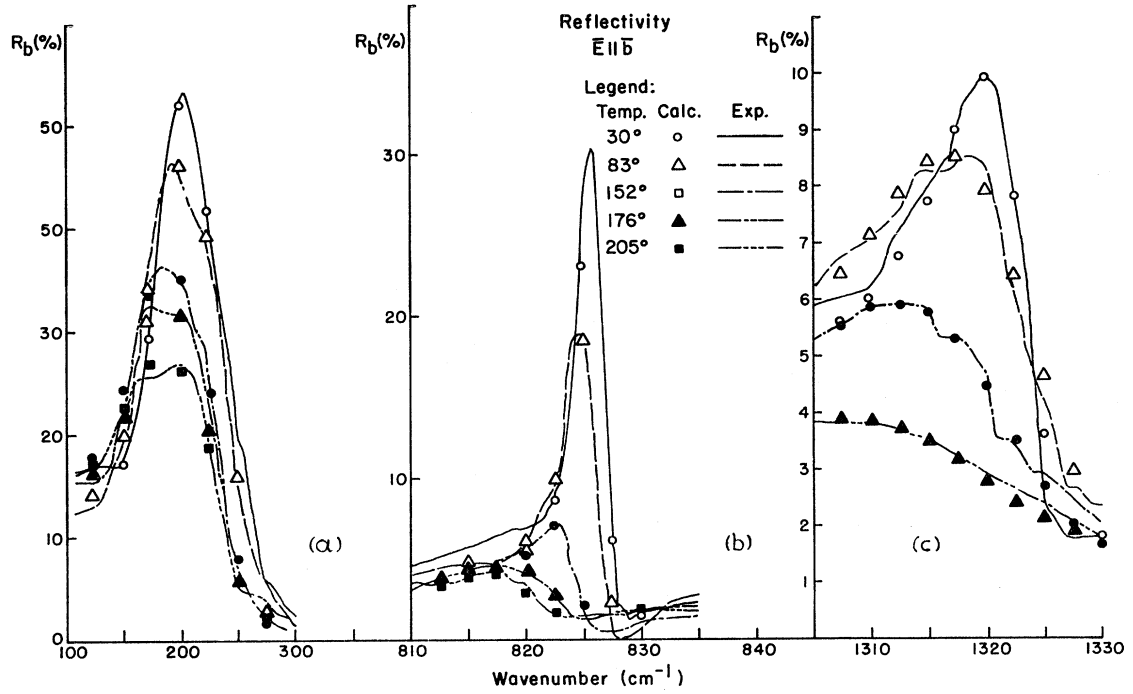

FIG. 3. (a) Temperature-dependent reflectivity of the translational lattice vibration active parallel to the polar b axis. The curves are experimental and the points are calculated from the independent oscillator model. (b) Temperature-dependent reflectivity of the symmetric-bending internal-vibration active parallel to the polar axis. The curves are experimental and the points are calculated. (c) Temperature-dependent reflectivity of the symmetric-stretching internal-vibration active parallel to the polar axis. The curves are experimental and the points are calculated.

small.[20] A Kramers-Kronig analysis of the reflectivity at all temperatures considered was performed. The real and imaginary parts of the dielectric response obtained at 176°C are shown in Fig. 5. The values of the peak in the dielectric conductivity $\sigma=\omega\epsilon''$ and the frequency at which this peak occurs are listed in Table II for all temperatures considered.

For a system of independent oscillators the complex dielectric response function as a function of wave number is given by[21]

$$\epsilon^*(\nu)=\epsilon'(\nu)+i\epsilon''(\nu)=\epsilon_\infty+\sum_{i=1}^{N}\frac{s_i}{(\nu_i^2-\nu^2)-i\Gamma_i\nu}. \quad (1)$$

Here N is the number of oscillators and ν_i, Γ_i, and s_i are the resonant frequency, damping constant, and strength of the ith oscillator, respectively. ϵ_∞ is a constant term which represents the contribution to the dielectric constant from electronic transitions which occur above 4000 cm^{-1}. Reflectivity is related to the dielectric constant by the Fresnel equation. Oscillator parameters were obtained using a computer program which calculates the reflectivity from Eq. (1) and simultaneously displays the calculated and experimental values on a cathode-ray tube. The parameters in Eq. (1) were then adjusted until a best fit to the experimental data was obtained as judged by visual comparison of the two curves. The fits obtained at 176°C are shown in Fig. 1. Initial parameters used were obtained from the results of the Kramers-Kronig analysis. The fit shown is typical of those obtained at all other polarizations and temperatures considered, portions of which are shown in Figs. 2–4 along with the experimental data. Parameters obtained from these fits are listed in Table II. In this table the quantity $\Delta\epsilon_i$ is the contribution of the ith mode to the low-frequency ($\nu\ll\nu_i$) dielectric constant; that is, substitution of $\nu\simeq 0$ in Eq. (1) results in

$$\epsilon'(0)-\epsilon_\infty=\sum_i\frac{s_i}{\nu_i^2}=\sum_i\Delta\epsilon_i. \quad (2)$$

Note that $\Delta\epsilon_i$ is equivalent to the integrated strength of the ith mode obtained from the Kramers-Kronig integral, that is,

$$\Delta\epsilon_i=\frac{2}{\pi}\int\frac{\epsilon_i''(\nu)}{\nu}d\nu,$$

where $\epsilon_i''(\nu)$ is the imaginary part of $\epsilon^*(\nu)$ associated with the ith mode.

In order to estimate the uniqueness of the parameters obtained by the visual-fit technique, a fit to the room-temperature reflectivity polarized along the a axis was attempted several times. The average percentage deviation of the parameters from their average values was found to be $\pm 1.2\%$.

[20] D. W. Berreman, Appl. Opt. 6, 1519 (1967).
[21] J. M. Ziman, *Principles of the Theory of Solids* (Cambridge University Press, New York, 1964).

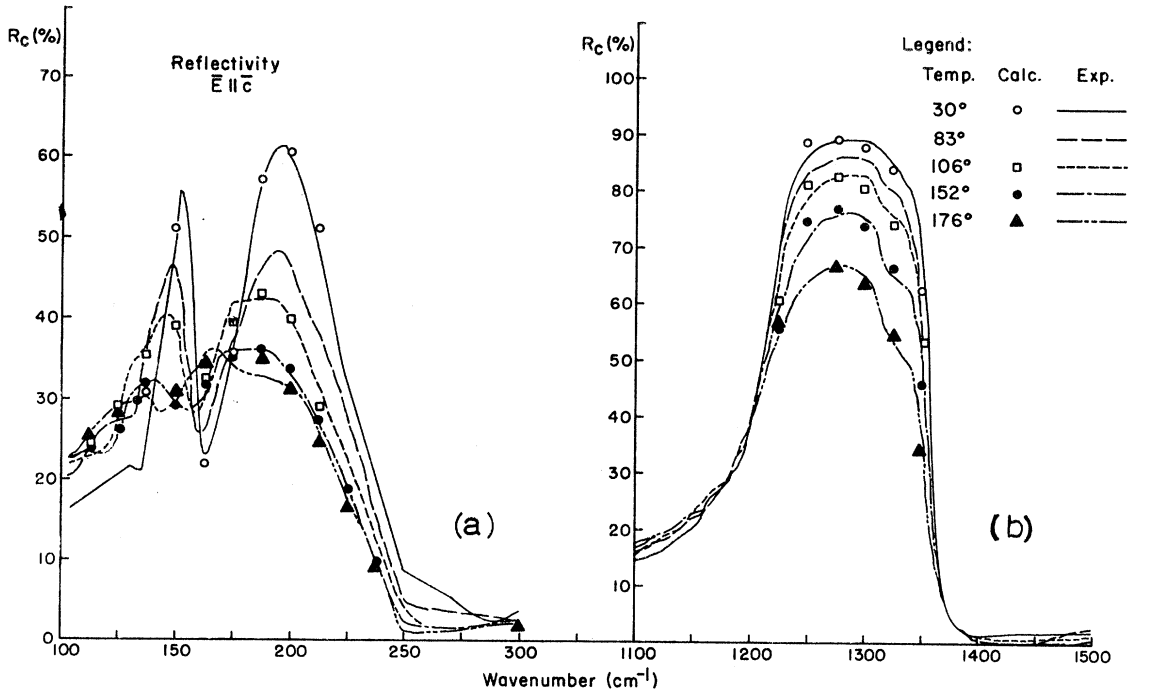

FIG. 4. (a) Temperature-dependent reflectivity of the two c-axis lattice modes of type B_1. The curves are experimental and the points are calculated from the independent oscillator model. (b) Temperature-dependent reflectivity of the asymmetric-stretching internal-vibration active parallel to the c axis. The curves are experimental and the points are calculated.

Low-frequency dielectric constants calculated from Eq. (2) are listed in Table III. The dielectric constants obtained in this manner were found to be only slightly temperature-dependent. Room-temperature values obtained from microwave measurements[18] are $\epsilon_a=5.2$, $\epsilon_b=4.18$, and $\epsilon_c=7.8$. The room-temperature values listed in the table are approximately 17% lower than the measured values. This lack of agreement might suggest that there exists additional dispersion between 100 cm^{-1} and the microwave region. However, due to the fact that all the normal modes predicted by symmetry are accounted for, any additional dispersion in the ferroelectric phase is not considered to be likely and was not observed experimentally between 10 and 70 cm^{-1}. It is quite clear that the infrared contribution $\epsilon'(0)$ is not large enough to cause the large anomalous temperature dependence of the low-frequency dielectric constant which has been observed,[1] that is, it appears that none of the eight infrared-active normal modes is a ferroelectric soft mode.

V. DISCUSSION

The temperature dependences of the resonant frequencies, linewidths, and strengths of all eight infrared-active modes can be obtained by inspection of Table II. If the values of the various mode parameters listed in the table are plotted as a function of temperature, it becomes apparent that the parameters associated with the translational vibration active parallel to the a axis exhibit anomalous behavior near the transition temperature. As the temperature is increased, the frequency of this mode decreases until the transition is reached. With a further increase in temperature the resonant frequency then begins to increase. In addition, both the linewidth and strength of this mode increase, with broadening becoming more pronounced near the transition temperature. On the other hand, the phase transition does not affect the parameters of the other lattice mode active parallel to the a axis, which appears to be normally behaved. The frequency and strength decrease slightly while the width increases with increasing temperature.

All modes active parallel to the polar b axis exhibit strong temperature dependence. Behavior of the translational A_1 lattice mode is similar to that of mode B_2 discussed above. Of the three internal modes, the symmetric bend active along the b axis is the most strongly affected in a narrow temperature interval around the phase transition. The frequency of this vibration decreases as the temperature is raised, the rate of decrease increasing considerably near T_c. Linewidth and mode strength show, respectively, increasing and decreasing trends with increasing temperature, with the former interrupted by a strong positive peak at the phase transition. The only notable facet of the temperature dependence of the other b-axis internal mode (symmetric stretch) is a considerable change in linewidth which has the same functional dependence on temperature as the b-axis symmetric bend discussed above.

Parallel to the c axis all modes are more normally

behaved and show similar changes, frequencies remaining fairly constant through the transition with each mode showing a general and strong increase in linewidth with increasing temperature. The strength of the internal vibration active in this orientation is constant, while that of the orientational lattice mode increases and that of the translational lattice mode decreases with increasing temperature. Upon inspection of the temperature-dependent reflectivity of the internal mode [Fig. 4(b)], a shoulder occurring at approximately 1325 cm^{-1} can readily be seen to be materializing as the temperature increases towards the transition temperature. This shoulder becomes less pronounced as the temperature increases beyond the transition. Due to the existence of this shoulder, the reflectivity cannot truly be fit with a single oscillator. No attempt to use an additional oscillator has been made at this time. It should be noted that the nonexistence of this shoulder at room temperature tends to rule out experimental polarization difficulties.

Symmetry of the atomic displacements of the internal symmetric bending vibration active parallel to the polar axis indicates that this mode is the one most likely to be effected by the disorder mechanism. Note that of the three internal vibrations of the nitrite ion, the oscillator parameters associated with this mode were the ones most profoundly effected by the phase transition. The two lattice modes which are most markedly effected by the phase transition are the translational vibrations active parallel to the a and b

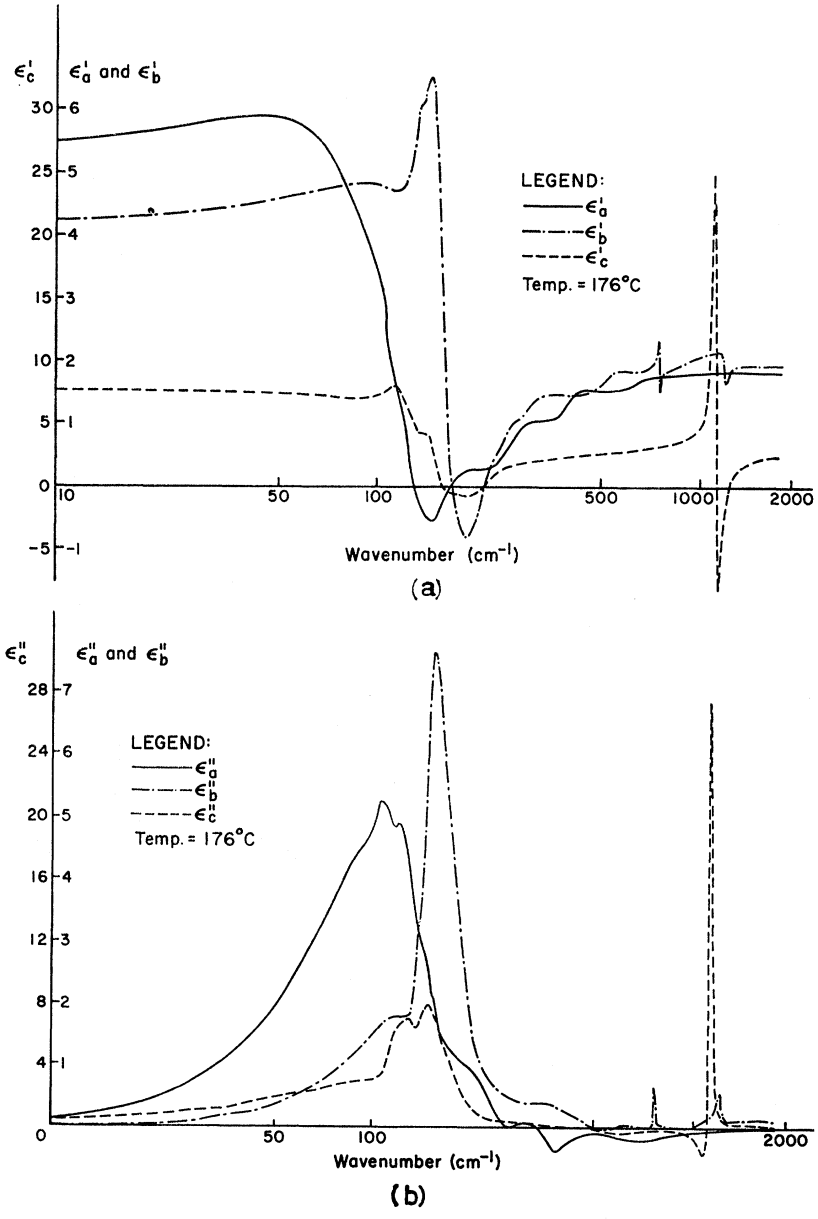

FIG. 5. (a) Real parts of the dielectric constants parallel to the three principal axes at a temperature of 176°C. The curves were calculated by Kramers-Kronig analysis of the data in Fig. 1. (b) Corresponding imaginary parts of the dielectric constant along the three principal axes.

TABLE II. Temperature dependence of dispersion parameters determined by Kramers-Kronig analysis and by fitting reflectivity with an independent oscillator model. In this table σ(max) is the peak in dielectric conductivity and ν is the frequency at maximum conductivity, both determined by Kramers-Kronig analysis. Parameters from the oscillator fit are S, the mode strength (multiply table value by 10^4); ν', the resonant frequency; Γ, the linewidth; and $\Delta\epsilon$, the mode contribution to low-frequency dielectric constant.

Temp. (°C)	σ(max) Mho/cm	ν cm^{-1}	$S\times10^{-4}$ $(cm^{-1})^2$	ν' cm^{-1}	Γ cm^{-1}	$\Delta\epsilon$	σ(max) Mho/cm	ν cm^{-1}	$S\times10^{-4}$ $(cm^{-1})^2$	ν' cm^{-1}	Γ cm^{-1}	$\Delta\epsilon$	σ(max) Mho/cm	ν cm^{-1}	$S\times10^{-4}$ $(cm^{-1})^2$	ν' cm^{-1}	Γ cm^{-1}	$\Delta\epsilon$
	$\bar{E}\|\bar{a}$ trans. vib. type B_2						$\bar{E}\|\bar{a}$ orient. vib. type B_2											
30	31.94	144	4.21	145.66	12.60	1.99	6.46	220	1.89	231.69	39.86	0.351						
83	29.60	143	4.33	144.14	18.42	2.09	7.0	215	2.16	224.82	58.46	0.427						
106	18.46	133	4.08	143.39	22.02	1.63	4.73	211	1.78	219.87	42.19	0.368						
152	15.97	128	4.57	133.80	42.70	2.55	4.81	210	1.63	220.04	56.57	0.337						
176	10.46	128	5.34	134.20	67.90	2.97	no peak	no peak	0.74	220.40	57.46	0.153						
205	12.39	135	5.08	141.75	69.48	2.53	6.87	213	1.15	220.40	63.00	0.236						
	$\bar{E}\|\bar{b}$ trans. vib. type A_1						$\bar{E}\|\bar{b}$ sym. bend type A_1						$\bar{E}\|\bar{b}$ sym. stretch type A_1					
30	38.84	186	4.93	186.82	20.83	1.41	84.46	825	0.656	825.25	1.44	0.00964	40.92	1321	2.10	1320.47	8.38	0.0121
83	42.00	183	5.37	179.47	31.28	1.67	43.51	824	0.674	824.12	2.54	0.00992	37.02	1318	4.00	1316.71	17.85	0.0231
152	16.08	163	6.31	171.72	48.13	2.14	18.56	823	0.390	823.20	3.41	0.00575	13.35	1320	2.89	1317.22	21.32	0.0167
176	21.40	169	5.60	172.17	49.00	1.89	8.99	821.5	0.597	820.24	8.84	0.00887	11.90	1316	2.00	1316.00	28.00	0.0115
205	12.12	160	6.59	173.25	68.14	2.20	7.0	820	0.262	819.19	5.50	0.00391	8.69	1327	1.56	1322.14	22.81	0.009
	$\bar{E}\|\bar{c}$ trans. vib. type B_1						$\bar{E}\|\bar{c}$ orient. vib. type B_1						$\bar{E}\|\bar{c}$ asym. stretch type B_1					
30	75.26	154	2.53	150.85	7.12	1.11	84.56	187	4.07	180.73	16.21	1.25	894	1223	79.7	1227.25	8.13	0.529
83	41.79	148	2.44	147.2	10.80	1.13	33.81	181	4.69	179.69	27.41	1.45	428.9	1216	81.82	1222.11	11.23	0.548
106	30.09	145	2.48	145.53	16.03	1.17	30.48	173	5.08	174.43	34.95	1.67	1144	1228	86.7	1227.92	14.96	0.575
152	19.01	142.5	0.775	141.16	12.96	0.384	23.68	170	7.84	172.73	53.38	2.60	1175	1235	85.9	1228.21	21.27	0.569
176	16.57	137	0.758	132.22	20.18	0.434	21.26	161	7.69	164.43	59.18	2.84	567	1229	78.9	1219.75	31.76	0.529

axes. The fact that the polar-axis mode exhibits anomalous behavior near the transition temperature is not surprising since the disorder occurs along this axis. Because the a-axis translational vibration is also effected by the phase transition while the c-axis modes are not, one can conjecture that the disorder mechanism is occurring about an axis parallel to the c axis. This conclusion is in agreement with previous NMR results[22] but is not supported by the Raman work of Chisler and Shur[23] nor by infrared depolarization measurements.[9] The primary temperature dependence of the remaining modes is in their linewidths. This is to be expected since both increasing temperature and increasing disorder as the transition is approached result in a greater phonon-collision rate. More detailed theoretical interpretation is in progress.

TABLE III. Low-frequency dielectric constants obtained from the independent harmonic-oscillator model via Eq. (2).

Temp. (°C)	$\epsilon_a(0)$	$\epsilon_b(0)$	$\epsilon_c(0)$
30	4.25	3.51	5.35
83	4.42	3.43	5.52
106	3.94		6.03
152	4.73	4.19	6.12
176	4.94	3.85	6.06
205	4.55	4.21	

[22] Unpublished work quoted in Ref. 9.
[23] E. V. Chisler and M. S. Shur, Phys. Status Solidi **17**, 173 (1966).

VI. CONCLUSION

Reflectivity of single-crystal sodium nitrite has been measured as a function of temperature and crystallographic orientation over a frequency region which spans all infrared-active vibrational modes. The dispersion of the dielectric constants has been obtained by Kramers-Kronig analysis and by fitting the data to a series of independent harmonic oscillators. It has been shown that the reflectivity of all eight infrared-active modes can be matched with that of a series of independent oscillators. It is also clear that the temperature dependence of the infrared active modes cannot account for the behavior of the low-frequency dielectric response near the transition temperature. Therefore, none of the eight infrared-active modes is a ferroelectric soft mode causing the phase transition. Three modes whose parameters show the largest anomalous temperature dependence are those whose symmetries are most closely connected with the change in lattice symmetry which occurs at the phase transition.

ACKNOWLEDGMENTS

The authors are pleased to thank the New York State Veterinary College, Physical Biology Computer Facility, which is supported by N.I.H. Grant No. FR-00326-2, for the use of its computer. We are also indebted to H. Moraff for constructive discussion associated with the visual curve-fitting programs.